EFDA–JET–PR(08)52

E. Andersson Sundén, H. Sjöstrand, S. Conroy, G. Ericsson, M. Gatu Johnson, L. Giacomelli, C. Hellesen, A. Hjalmarsson, E. Ronchi, M. Weiszflog, J. Källne, G. Gorini, M. Tardocchi, A. Combo, N. Cruz, A. Batista, R.Pereira, R. Fortuna, J. Sousa, S. Popovichev and JET EFDA contributors

The Thin Foil Magnetic Proton Recoil Neutron Spectrometer MPRu at JET

The Thin Foil Magnetic Proton Recoil Neutron Spectrometer MPRu at JET

and JET EFDA contributors*
E. Andersson Sundén, H. Sjöstrand[1], S. Conroy[1], G. Ericsson[1], M. Gatu Johnson[1], L. Giacomelli[1, 6], C. Hellesen[1], A. Hjalmarsson[1], E. Ronchi[1], M. Weiszflog[1], J. Källne[2], G. Gorini[3], M. Tardocchi[3], A. Combo[4], N. Cruz[4], A. Batista[4], R.Pereira[4], R. Fortuna[4], J. Sousa[4], S. Popovichev and JET EFDA contributors*

JET-EFDA, Culham Science Centre, OX14 3DB, Abingdon, UK

[1]Uppsala University, Department of Physics and Astronomy, 751 20 Uppsala, Sweden (EURATOM-VR)
[2]Uppsala University, Department of Engineering Sciences, 751 21 Uppsala, Sweden (EURATOM-VR)
[3]Physics Department, Milano-Bicocca University, and Istituto di Fisica del Plasma del CNR, Milan, Italy (EURATOM-ENEA-CNR)
[4]Centro de Fusão Nuclear, Instituto Superior Técnico, Av. Rovisco Pais 1, 1049-001 Lisboa, Portugal (EURATOM/IST,)
[5]EURATOM-UKAEA Fusion Association, Culham Science Centre, OX14 3DB, Abingdon, OXON, UK
[6]Now at Physikalisch-Technische Bundesanstalt (PTB), Fachbereich 6.5, D-38116 Braunschweig, Germany
** See annex of M.L. Watkins et al, "Overview of JET Results",*
(Proc. 21 st IAEA Fusion Energy Conference, Chengdu, China (2006)).

Preprint of Paper to be submitted for publication in
Nuclear Instruments and Methods in Physics Research Section A

ABSTRACT.
Neutrons are produced in fusion energy experiments with both Deuterium (D) and Deuterium - Tritium (DT) plasmas. Neutron spectroscopy is a valuable tool in the study of the underlying fuel ion populations. The Magnetic Proton Recoil neutron spectrometer, originally installed at JET in 1996 for 14MeV neutron measurements, has been upgraded, with the main aim to improve its Signal-to-Background ratio (S/B), making measurements of the 2.5MeV neutron emission in D plasmas possible. The upgrade includes a new focal plane detector, based on the phoswich technique and consequently less sensitive to background, and a new custom designed digital data acquisition system based on transient recorder cards. Results from JET show that the upgraded MPRu can measure 2.5MeV neutrons with a S/B = 5, an improvement with a factor of 50 compared to the original MPR. A S/B of 1.4×10^4 in future DT experiments is estimated. The performance of the MPRu is exemplified with results from recent D plasma operations at JET, both concerning the new 2.5MeV measurements with Ohmic, RF and NB heating, as well as 14MeV measurements of tritium burn-up neutrons. The upgraded instrument allows for 2.5MeV neutron emission and deuterium ion temperature measurements in plasmas with low levels of tritium, a feature necessary for the ITER experiment.

1. Introduction

Neutrons (n) are produced in fusion energy experiments in Deuterium (D) plasmas through the reaction $d + d \rightarrow {}^3He + n$ ($E_n = 2.5MeV$) and in Deuterium-Tritium (DT) plasmas through d+t!í±+n ($E_n = 14MeV$). Neutron Emission Spectroscopy (NES) is a valuable tool in fusion energy research, since the neutrons leave the fusion plasma undisturbed and can give information on the state of the fuel ions and thereby on important plasma parameters. NES often focuses on measurements of the dominant 2.5MeV or 14MeV neutron emission and phenomena such as ion kinematics, alpha knock-on (1) and plasma heating (2) (3) are studied. However, measurements of the minority-energy emission are also of interest, e.g., the 14MeV neutrons from tritium burn up in D plasmas (4) and 2.5MeV neutrons in DT plasma operations; the latter being of particular significance as it would allow an estimate of the density ratio, n_d/n_t. Measurements of the 2.5MeV neutron flux in a substantial 14MeV neutron background is a requirement for ITER D operations. The high power of the ITER pulses in combination with long particle confinement times will lead to the build-up of a tritium inventory from $d + d \rightarrow t + p$ reactions (5). DT reactions involving this accumulated tritium will contribute to a strong 14MeV neutron source.

The measurement conditions close to a fusion reactor are harsh. High levels of background radiation of neutrons and gammas are often present and the stray magnetic field from the fusion machine (tokamak) is a further complication. In addition, for machines like ITER, temperatures close to the vessel are predicted to be high. Ideally, a fusion neutron spectrometer should be able to handle both a high variability in count rate, reflecting transients in the underlying plasma conditions, a high level of background radiation as well as the other adverse environmental conditions. In the

design of a spectrometer for plasma neutron measurements a number of performance indicators need to be taken into account; which depends on the intended application. These performance indicators include: the instrument's sensitivity, i.e., the ability to measure weak components in the neutron emission; the rate capability of useful counts in the spectrum; the energy bite, i.e., the energy range covered by the instrument; the operational and calibration stability; the energy resolution; and the efficiency. Furthermore, the system should possess a flexibility (or inherent capability) to cope with neutrons in a broad band of energies, specifically around 2.5 and 14MeV, and in a wide range of neutron emission intensities (dynamic range). In addition, interfacing issues might be a concern, especially for instruments of considerable size and/or with particular installation requirements.

JET has explored and developed NES since the early 1980's (6). The Magnetic Proton Recoil spectrometer (MPR) concept was conceived in the early 1990's (7) and a first spectrometer of this type was installed at JET in 1996 and has been in operation in all subsequent campaigns (1) (2) (3) (4) (8) (9) (10). The original MPR was optimised for measurements of the 14MeV neutron emission in high power DT plasmas and designed to provide efficient background rejection in order to discern and determine the weak components of the spectrum. The design was also flexible enough to allow for measurements of the 2.5MeV neutron emission, although these measurements were severely hampered by a high background level (11). In the 14MeV case, the MPR has been operated at a maximum signal count rate of 0.61 MHz with a signal-to-background ratio (S/B) of $2 \cdot 10^3$. The 2.5MeV neutrons emitted from D plasmas were measured with a S/B=10^{-1}. (11)

The MPR has been upgraded (12) (13) as part of the JET enhanced performance programme, JET-EP1 (14). The emphasis of the upgrade has been on the spectrometer's focal plane detector, the associated data acquisition and the control and monitoring system. Some subsystems like the conversion foils and the vacuum system have also seen substantial changes. However, the upgraded spectrometer also retains many of the original components, e.g., the neutron collimator, magnetic system, proton collimator and radiation shield. The aim of the MPR upgrade project was to improve the S/B for 2.5MeV neutron measurements in D plasmas by a factor 100 and a factor of 10 in 14MeV DT plasmas, while retaining the high count rate capability of the system.

The MPR upgrade (MPRu) instrument is described in this paper. Section 2 introduces the measurement principles of the device and the requirements that have to be met for measurements of both 2.5MeV and 14MeV neutrons. Section 3 reviews the technical and mechanical solutions adopted for the different subsystems of the device and section 4 describes their operational working points. Section 5 gives a brief description of the installation of the MPRu at JET, both physically and in terms of data acquisition and data transfer. Section 6 presents some results on calibration and performance. Finally, discussion, outlook and conclusions are given in Sections 7, 8 and 9.

2. MEASUREMENT PRINCIPLES AND REQUIREMENTS

The MPRu is based on the thin-foil proton recoil technique employing a magnetic field for the momentum (energy) separation of the recoil protons (p). Collimated neutrons impinge on a thin

foil, where a small fraction of the neutrons undergo elastic nuclear scattering on hydrogen nuclei (protons). The energies of the recoil protons are

$$E_p = E_n \cos^2\theta_{np} \tag{1}$$

where E_p is the proton energy, E_n is the incoming neutron energy, and θ_{np} is the scattering angle in the lab system. A circular aperture selects forward scattered protons. By selecting protons in the forward direction the np cross section is maximised as is the recoil proton energy, resulting in an improved S/B of the detector. The selected protons enter a magnetic system where they are momentum analysed. Finally, the positions of the protons are actively measured in a position sensitive scintillator array placed in the curved focal plane of the magnet. The application of particle transport in a magnetic field makes it possible to avoid some of the problems associated with placing energy-resolving detectors in or close to the collimated neutron flux.

As mentioned above, the requirements on a high-resolution neutron spectrometer for fusion applications depend partly on the intended application, i.e., on the plasma parameters that one wants to study. It has been the ambition of the MPRu development to design an instrument to explore the full potential of neutron spectroscopic measurements in high power fusion plasmas of both D and DT fuel.

3. COMPONENTS OF THE MPRU SYSTEM

The original MPR design and installation has been described in some detail before (7) (8). Since the measurement principle of the system has not changed, we give only a brief summary here. A schematic overview of the MPRu system is shown in Figure 1. Plasma neutrons pass through a neutron collimator forming a neutron "beam" into the spectrometer. At the end of the collimator, the neutron beam intersects a thin polythene (CH_2) foil target where some neutrons scatter elastically on the protons (hydrogen nuclei) of the foil. A circular aperture, serving as proton collimator, selects the forward scattered protons, which then enter the magnetic system where they are spatially separated according to their momentum.

The magnetic system consists of three main parts; the coils energising the magnet; the magnetic pole pieces shaping the magnetic field to its desired topology; and finally the yoke, which also serves as vacuum vessel and magnetic shield against JET's strong stray field.

A detector array of scintillators is placed at the curved focal plane of the spectrometer, detecting the positions of the momentum separated protons. The MPRu scintillators are of phoswich type (15).

The spectrometer is surrounded by a concrete radiation shield further complemented with lead closest to the focal plane detector. Neutrons that pass through the thin target foil are stopped in a beam dump located in the far wall of the radiation shield to avoid scattering of neutrons into the spectrometer and towards the detector.

The MPRu's ion optical system is designed for the neutron'"beam" to be aligned along a specific

axis through the instrument, here referred to as the optical axis (straight line through the neutron collimator in Figure 1). For optimal performance, all physical components have to be accurately aligned and positioned with respect to this axis. Specifically, this concerns the neutron collimator, the conversion foil, the proton collimator and the focal plane detector. The extended optical axis towards the JET machine defines the centre of the field of view, i.e., the Line Of Sight (LOS), of the instrument."

3.1 NEUTRON COLLIMATOR

The neutron collimator defines the neutron "beam" entering the MPRu and the field of view into the plasma. The collimator is partly integrated within the concrete radiation shield facing the torus (Figure 1). It consists of two steel cylinders, each of length 350mm, outer diameter 150mm and with a concentric bore of $10cm^2$. Both cylinder bores are aligned to the optical axis by optical surveying, by the use of a theodolite. The inner cylinder is fixed to the spectrometer yoke, at a distance of 0.17m from the foil, while the plasma-facing outer cylinder can move relative to the inner one to a position 1.3m towards the plasma, allowing for a flexible effective collimator length in the range 0.87m to 2.17m.

The position of the movable, outer cylinder is set by a remotely controlled motor. The number of revolutions made by the motor is monitored to give the cylinder position and thereby the collimator length. Micro-switches are installed at the extreme cylinder positions to prevent the motor from driving the system beyond its limits.

3.2 CONVERSION FOILS

A neutron-to-proton np conversion foil is placed at the end of the neutron collimator, inside the MPRu vacuum chamber and aligned to the optical axis. Six different circular foils are installed in a special foil-holder arrangement. The foils are 10 cm^2, chemically pure, self-supporting CH_2 targets[1] with different thicknesses to accommodate different operating scenarios in both 2.5 and 14MeV neutron measurements (Table 1). The foil holder is a wheel-like construction (Figure 2) made mostly of aluminium but with the parts closest to the neutron beam, facing the spectrometer, made of graphite in order to reduce the risk for undesired np scattering events in the holder mechanics[2]. The assembly is about 150mm across.

The thickest conversion foil has a small central circular cut-out and a cross-hair installed (on the plasma-facing side) for alignment purposes. A motor placed outside the vacuum chamber controls the selection of conversion foil; the motor is stopped by micro switches at the six positions that place the conversion foils in positions aligned to the optical axis (neutron beam). A long straight shaft with a vacuum tight feed-through connects the motor to the centre of the foil wheel.

3.3 PROTON COLLIMATOR

The proton collimator is aligned with the optical axis and selects forward scattered protons from the conversion foil for further analysis in the spectrometer's magnetic field. It is tilted with 15

[1] *Provided by Goodfellow, Huntingdon, Cambridgeshire, England, and Borealis AS, Stathelle, Norway*
[2] *The threshold for np reactions in Carbon is high, about 12MeV, while it is only 1.8MeV in Aluminum*

degrees with respect to the target foil as required by the bending of the proton trajectories at this point. The proton collimator arrangement consists of two components, namely, a 2mm thick collimator "wheel" (Figure 2) attached to a 3mm thick screening plate. The collimator wheel has five triangular holes onto which up to five 3mm thick "pie" pieces, defining more restrictive circular apertures, can be attached. The sizes and shapes of the presently installed apertures are given in Table 2. The collimator wheel is 230mm in diameter.

The wheel is controlled by a motor, placed outside the vacuum chamber, and stopped by micro switches at the five aligned positions. The motor turns the wheel so that the desired aperture is placed in front of a hole in the screening plate. The screening plate is attached to the front of the D1 poles and has a single fixed opening corresponding to the largest opening in the collimator wheel, i.e., the triangular one of position 2 (Figure 2). The screening plate allows only protons with trajectories through the selected aperture to reach the magnetic part of the system. One of the apertures has a cross hair installed, used in the alignment of the collimator..

3.4 ELECTROMAGNET AND INTEGRATED PARTS

The momentum (energy) separation of the protons is performed passively in the spectrometer's magnetic field. The MPRu electromagnet system consists of the yoke, the coils, the pole pieces and the integrated monitoring equipment. The magnetic return yoke is an irregularly shaped steel box (Figure 1) with approximate outer dimensions (L×H×W) 1.50m × 2.25m × 0.80m and a wall thickness of 0.20 m. It surrounds the magnetic volume, thereby preventing all but a small (a few Gauss just outside the yoke) stray field to leak out into the surrounding area even at the highest magnetic excitation levels. The yoke also serves as magnetic shield against the strong stray field produced by the tokamak, which can reach several hundred Gauss at the spectrometer's position on JET. Larger penetrations in the yoke are provided for neutron beam entrance and exit, for protons exiting to the focal plane detector and for cooling water and power services to the coils. Two smaller penetrations are provided for the motor driving shafts of the foil and collimator wheels.

The electromagnet is energised by two sets of D-shaped coils, which are manufactured from about 1km of insulated rectangular copper pipes with centred circular holes for water cooling. The coils are powered by a Magnetic Power Supply (MPS) providing a maximum current of 560 A at 105V voltage drop. The MPS is placed in the JET basement below the spectrometer and is remotely controlled and monitored.

The magnetic field (Figure 3) is given its shape from two separate poles, one multi pole, D1, and one pole of clam-shell design, D2. The two parts of the D1 pole are each built up from 11 plates of individual profiles while the two pieces of the D2 pole are manufactured from single blocks of metal. The D1 produces a field with strong multi-pole components. These components, mainly of quadru- and sextupole type, give focusing of the protons in the momentum-dispersive direction of the magnet and provide higher-order ion-optical corrections. The D1 bends the protons by about 30 degrees and produces a field with strong multi-pole components. The D2 bends the protons an

additional 120 degrees while also assisting in the focusing. The curved entrance and u-shaped exit boundaries of the D2 provide further ion optical corrections.

Three magnetic field probes (Hall probes) are placed in the spectrometer for monitoring of the magnetic field; one in each magnetic pole and one at the focal plane detector. Together with the measured field maps (see Section 6), these monitors provide the information needed to determine the magnetic field topology for any excitation level. The Hall probes are also used to monitor the stability of the B-field and the temperature at their locations; they are read out at a frequency of 4Hz during plasma operation. Additional temperature probes (Pt100) are placed on the cooling water pipes for the coils to monitor any temperature fluctuations. Water flow guards are also installed on the cooling water pipes both on the electro-magnet and on the MPS; in the event of a drop in water pressure these units switch off the MPS.

The spectrometer is equipped with a local vacuum system, serving the one cubic meter volume enclosed by the yoke and the extension box housing the focal plane detector. The pressure is kept at a level of typically 10^{-4} mbar, which is low enough to prevent energy loss and scattering of the recoil protons to significantly affect the measurements. The vacuum components consist of a turbo and a backing pump, connected via a remotely controlled valve, and two vacuum gauge heads with associated read out electronics, also controlled remotely. The turbo pump is directly attached to the spectrometer's vacuum vessel in the beam dump region, well removed from the neutron beam. It connects to the backing pump via a flexible tube pulled through a curved channel in the back wall of the radiation shield. In addition, a sliding 50μm thick steel vacuum window is installed at the spectrometer entrance, remotely controlled by compressed air. This seal can be opened for LOS surveying. The vacuum flange at the exit of the neutron beam is also accessible from the outside, by removing the beam dump plug in the shielding back wall.'

3.5 FOCAL PLANE DETECTOR

The core of the MPRu focal plane detector is a 32-element array of phoswich scintillators. Each scintillator has two Photo-Multiplier Tubes (PMTs) attached. The detector can be divided into three parts; the detector mechanics, the scintillator array and the PMT assemblies. The detector mechanics serves both as the mounting frame for the PMTs and the phoswich scintillators as well as magnetic shield of the PMTs; it also assists in the heat dissipation of the PMT bases. The focal plane of the magnetic system is curved in space (see Figure 3). For simplicity, the focal plane detector has been constructed as a single straight plane.

3.5.1 Phoswich detectors

The phoswich scintillators[3] consist of two scintillating layers in optical contact, each with its characteristic light-pulse decay-time. A thin (0.3mm) layer with a short decay time (t_{decay} =1.8ns, material Bicron BC404) faces the incoming protons, followed by a thick (2.3–3.2mm) layer with a long decay time (t_{decay} =180ns, Bicron BC444) and finally a backing layer (0–5mm) of the same

[3] *Provided by St. Gobain (Bicron), Newbury, Ohio, US.*

material as the light guides (Bicron BC800). The range of 2.5MeV and 14MeV protons in scintillator plastic is about 0.1mm and 2.2mm, respectively. Hence, a 2.5MeV proton is stopped in the thin layer whereas a 14MeV proton deposits its energy in both scintillator layers. This results in different pulse shapes depending on proton energy (and particle type), a property of the phoswich detectors that is exploited here to improve the background rejection.

Phoswich scintillators of four different types are mounted in the detector, labelled III, IV, V and VI for historical reasons. Types III and VI are 20mm wide, used in the low and high energy sections of the detector plane, and have straight light guides. Types IV and V are narrower (10mm), have bent light guides, and are placed in the central section. Types IV and V differ only in the bending direction of the light guides, being bent either towards or away from the electromagnet. (See Table 3 and Figure 4) (12).

The light guides transform the rectangular shaped phoswich (and backing) cross section to a circular one suitable to couple to the PMT.

The thickness of the thin layer is purposely chosen to be substantially larger than the range of 2.5MeV protons in plastic. This is to ensure sufficient energy deposition for penetrating 14-MeV protons in this layer; there are manufacturing advantages as well.

To give good optical coupling the light guides at each end of the phoswich scintillators are connected to the PMTs via 3 mm thick cylindrical silicon pads to which a thin film of optical grease have been applied.

The available space in the detector location is restricted. The use of two PMTs per scintillator therefore required some changes of the system. Such changes included the increase of the width of the central channels (from 8mm to 10mm), the bending of the light guides of the central channels, and the reduction in the number of detectors in the detector array (from 37 to 32).

3.5.2 PM-tube assemblies

Each phoswich detector is attached to two PMTs[4] for a total of 64 installed. The PMTs have an outer diameter of 19 mm and a length of 127 mm as measured from the photocathode to the back. The bare glass PMT is coated with a conductive layer, sleeved with an insulator, and fitted within a 0.2 mm μ-metal cylinder for magnetic shielding. The photocathodes have an active area with diameters in the range 14.7–17.6mm and quantum efficiencies between 24.6% and 34.0%. For typical 14MeV proton induced pulses, the PMT resistor chain is designed to give a maximum gain shift of 6% at a count rate of 100 kHz. Such rates are a concern only in high power DT operations; in D operation rates are expected to be sufficiently low to avoid any rate-dependent effects. The PMTs are long-term vacuum compatible and designed to each generate less than 1 W of heat at nominal high voltage (–1500V). Two remotely controlled High Voltage (HV) power supplies[5] provide the necessary high voltage for the PMTs, in the range –1000V to –1600V.

The temperature in the surroundings of the PMTs is measured by two Pt100 elements, one in each PMT box (see below).

[4] *Provided by Electron Tubes Ltd, Ruislip, UK. Assembly type P19VN-06.*
[5] *Provided by CAEN, Viareggio, Italy.*

3.5.3 Magnetic shielding and mechanics

The MPRu system is sensitive to magnetic field disturbances. This concerns, firstly, the ion optical properties of the spectrometer, which are determined by the magnetic field topology as provided by the D1 and D2 poles. Consequently, the magnetic volume must be shielded from any external magnetic field; this is provided by the thick walls of the electromagnet's return yoke. Secondly, the PMTs must be shielded to sub-Gauss levels to function properly. Therefore, the PMT magnetic shield consists of three layers. The outermost layer is a 20mm thick soft iron cap surrounding all sides of the detector installation volume except the side facing the electromagnet and an opening below the detector for feed-through of signal and HV cables. The next layer, the PMT mounting boxes of the detector mechanics (Figure 5), is manufactured from 4mm thick soft iron and, finally, each PMT is enclosed in a 0.2mm thick μ-metal cylinder.

A Hall probe for magnetic field measurements is placed inside one of the PMT boxes. The field is monitored during plasma operations and has been shown to be unaffected (within 0.1 Gauss) by the operations of the tokamak magnetic field for all JET operational scenarios as well as by the operations of the spectrometer's electromagnet up to its maximum excitation. The remaining magnetic field in this area is at a sufficiently low level to be safely handled by the PMT's º-metal shield.

The position of the assembled focal plane mechanics relative to the components of the magnetic system has been measured by 3D photogrammetry with an uncertainty of 0.05mm (16). The width and position of each scintillator in the MPRu detector array were measured by illuminating the scintillators of the fully assembled hodoscope with light from a pulsed ultraviolet LED light source. The relative positions of the scintillators were determined with an uncertainty of 0.05mm (17).

The PMTs are placed in aluminium holders to improve the heat dissipation from their voltage divider bases. Still, temperatures during assembly (room temperature around 20^{o}C) are quite different from those at full operation of the magnet and detector (up to 60^{o}C). Therefore, two robust plastic bars and a plastic "roof", with the same heat expansion coefficient as the scintillators, have been inserted between the two PMT boxes (see Figure 5). One PMT box is free to move relative to the other one. With this arrangement, temperature variation causes the plastic to expand or contract at the same rate as the scintillators, thereby relaxing any stress on the scintillators.

For each phoswich scintillator, a light fibre is guided through a penetration in the plastic roof and directed perpendicularly to the back of the scintillator surface. Light emerging from the fibre is aimed at a spot (d~2 mm) of diffuse white paint applied on the opposite surface of the scintillator. This scatters the incident LED light randomly within the scintillator, and hence partly also towards the PMTs.

3.6 RADIATION SHIELD

Being placed in the JET torus hall, the MPRu is exposed to high levels of both direct and ambient gamma ray and neutron background radiation. The primary background source is the fusion plasma, emitting neutrons at predominantly 2.5MeV and/or 14MeV energies in all directions. The energy

distribution of the background is smeared out and shifted toward lower energies due to scattering in surrounding materials. The gamma rays are mainly due to capture of thermal neutrons in construction materials, for the MPRu mainly in its own radiation shield.

The radiation shield consists of seven large concrete blocks, in total weighing 60 tonnes, with an additional lead block of 2 tonnes around the focal plane detector for enhanced gamma suppression. Furthermore, the plastic roof in the focal plane mechanics shields from Compton electrons. The concrete shield wall that faces the plasma is 1.5m thick and the other walls are 0.50-0.76m. The larger voids between the magnet yoke and the concrete shield are filled with bags of polythene pellets for additional shielding. The same type of pellets is inserted into the void between the neutron collimator housing and the concrete. The concrete pieces were cast sequentially "in situ" from the bottom up, so that all joining horizontal surfaces were individually matched to each other. Thus, the shield gaps normally associated with the tolerances required by more traditional labyrinth-type joints were largely avoided and a practically seamless shield was obtained.

Signal and control cables are pulled out from the spectrometer past the shield through a hole in the lower back wall. The same hole is also used for the water and current cables for the electromagnet. A separate penetration in the upper back wall allows for the exhaust of the turbo pump (placed inside the concrete shield) to be connected to the backing pump (outside). The present shield configuration was designed and evaluated using a MCNP (18) model for the MPR and the JET torus hall.

3.7 BEAM DUMP

The neutron beam exiting the yoke is made to intersect with a hydrogen-rich plastic cylinder placed in a cut-out hole in the back concrete wall of the MPR. This beam dump is there to prevent the exiting neutrons from scattering back into the spectrometer where they could contribute to the background in the focal plane detector. The plastic plug is removable from the outside making access to the back exit vacuum flange of the spectrometer possible.

3.8 DATA ACQUISITION ELECTRONICS AND CONTROL AND MONITORING

The recoil protons interacting in the phoswich detector elements provide the primary signals on which the physics analysis in terms of neutron energy spectra is based. The MPRu signal processing chain, from phoswich scintillators to data storage in the system's intermediate data acquisition computers is shown in Figure 6. For each phoswich detector, it consists of two PMTs, a Pulse-Summing Amplifier (PSA), a channel in a Transient Recorder Card (TRC) (19) and associated cables. The phoswich scintillator placed at the very low energy end of the array (channel 0) serves some further functions in the Control and Monitoring (C&M) system and therefore has some additional components included in its signal processing chain; this is the situation depicted in Figure 6. The signals from the two PMTs connected to a phoswich detector are summed and amplified in the custom-built PSA. An amplification of about a factor of six is provided in order to match the

input range of the TRCs. The TRCs digitise and store the full pulse shape of the summed PMT signals. The input voltage range of the TRCs is 0 to -1 V over 50Ω and the digitisation is done with 8 bit resolution at 200 MHz sampling frequency. Each TRC has four input channels. The TRCs allow for individual settings for each channel regarding, e.g., voltage offset, trigger level, and the number of pre- and post trigger samples.

The C&M system consists of a number of artificial, controlled light sources (CLS) and in addition two scintillators with embedded sources for absolute reference. These latter light sources employ scintillators of the type Yttrium Aluminium Perovskite doped with Cerium (YAP:Ce) with embedded 5.5 MeV α-emitting ^{241}Am sources[6]. The YAP sources illuminate the photocathode of the two PMTs of the system's monitoring channel (channel 0). The light from a CLS is optically connected to the centre of every scintillator via light fibres. Two CLSs are installed with the MPRu, namely, a laser emitting green light (20) and a LED emitting blue light (21). To relate the time trace of the data from the spectrometer to that of JET, a 1 Hz standard NIM clock pulse is provided by JET and has been added to the signal chain of the monitoring channel via a Fan In/Fan Out (FIFO) unit.'6 Provided by Scionix, Bunnik, The Netherlands,

Pulses due to the YAP, the CLS and the clock have distinct shapes and, in some cases, fixed repetition frequencies, making them easily distinguishable from each other and from pulses due to particles interacting in the scintillators. The recording of the full pulse shape for each event with the [7] The standard deviation (√) is used since it is a function of the entire proton distribution. In contrast, the more frequently used Full Width Half Maximum excludes possible tail effects of the proton distribution. TRCs gives the possibility to perform off-line pulse shape discrimination and data reduction, as is discussed below.

4. SETTINGS OF OPERATIONAL POINTS

Different spectrometer working points are used to measure the 2.5MeV or 14MeV neutrons. Each working point is built up of the individual settings of the different spectrometer sub-systems. These include the length of the neutron collimator, the thickness of the np conversion foil, the aperture of the proton collimator, the magnetic field, the focal plane detector settings, and the data acquisition parameters employed.

4.1 OPTIMISATION

A characteristic of the thin-foil method is a reciprocal relation between energy resolution and efficiency. While the best resolution of the system is obtained when a thin conversion foil and a restrictive proton collimator aperture are used, the best efficiency requires the opposite choices.

The separation of tasks with the MPR technique offers the possibility to maximise the efficiency for a specific resolution by varying the settings of proton collimator aperture and conversion foil thickness. The two contour plots in Figure 7 show the results of a study to find the optimal working point for mono-energetic 14MeV neutrons. The figures show contours of efficiency and resolution

[6] *Provided by Scionix, Bunnik, The Netherlands*

(σ/E_n)[7] as a function of the foil thickness and the proton collimator radius. For a specific "choice" of resolution there is one combination of conversion foil thickness and proton collimator radius that maximises the efficiency. The set of optimised combinations is indicated by the thick red curve in the two panels of Figure 7. The neutron collimator length, the foil area, and possibly other parameters, can be included in this optimisation; here the foil area is 10 cm^2 and the neutron collimator length is 870mm. The B-field is 1.091T.

In practice, the MPRu is limited to three proton collimator radii and six conversion foil thicknesses. As can be seen in Figure 7, the setting actually installed is close to optimised for the 13.6mg/cm^2 foil while the situation for the 8.0mg/cm^2 is a bit less optimal. The configuration 8.09mg/cm^2 foil and proton collimator radius 34.9mm was the reference setting for good resolution operations in 14MeV of the original MPR. This setting was kept for backwards compatibility even though the optimisation calculation of Figure 7 indicates that a choice of ~10.0mg/cm^2 and 32mm would have been better for this particular choice of resolution.

The same optimisation is presented for the 2.5MeV case in Figure 8. Two of the installed foils are suitable for operations in the 2.5MeV energy region. The B-field is 0.4293T. As can be seen, the best operational points available, employing the largest installed proton aperture, of 40mm radius, are not very close to the optimal values. However, a proton aperture of R = 55mm, as suggested by this study, was not possible within the constraints given by the overall proton collimator mechanics. The neutron collimator is typically set to the minimum length, 870mm, to get the maximum number of neutrons impinging on the target. A longer collimator (resulting in a narrower viewing cone into the plasma) gives a somewhat improved energy resolution at the expense of reduced count rate." The magnetic field of the MPRu for 2.5MeV and 14MeV neutron measurements is about 0.4 T and 1.0T, respectively, but the field can in principle be set to accept any neutron (proton) energy in the range 0-18MeV. To achieve good reproducibility in the magnetic field setting the current is "cycled" to the desired value. This is done by slowly oscillating the current delivered by the MPS around the final value and decreasing the amplitude of the oscillation, until the desired setting is reached."

The only detector settings are the high voltage (HV) settings of the PMTs. The main issue of the HV settings is to provide the largest possible pulse height considering the HV limits of the PMTs and the -1V input maximum of the TRCs. A HV of a PMT also needs to be balanced with its partner tube of the same scintillator (22).

The CLS of the C&M system can also be set to different working points; in particular the LED can be set in numerous ways. For example, the operating frequency of the LED driver can be set between 20Hz and 20MHz and the width of the LED pulse can be adjusted in a wide range, from a few ns up to several hundred ns (21). Each TRC channel has a number of parameters that can be set to suit the application.

5. INSTALLATION AT JET

The installation of the MPRu in the JET torus hall is schematically depicted in Figure 9. The MPRu

[7] *The standard deviation (√) is used since it is a function of the entire proton distribution. In contrast, the more frequently used Full Width Half Maximum excludes possible tail effects of the proton distribution.*

views the plasma through a diagnostic port at about 4 m distance from the conversion foil. For a typical 2.5MeV and 14MeV plasma, the foil area of the MPRu is hit by the fraction $8 \cdot 10^{-9}$ and $9 \cdot 10^{-9}$ per JET neutron, respectively. The difference between the two cases is mainly due to attenuation effects. The fractions are referred to as the installation geometry factors. The LOS is semi-tangential passing through the plasma centre twice and making an angle of 47^{o} to the toroidal B-field at the plasma centre. To achieve the best possible coverage of the plasma, the LOS inclination is 4.8^{o} with respect to the equatorial plane of the tokamak (23).

5.1 DATA HANDLING, STORAGE AND REDUCTION

5.1.1 Data acquisition

The TRCs and other data collecting devices are connected to two Aata acquisition (DAQ) PCs. Both PCs are running a custom-built server program, using a HTTP 1.1 protocol. During plasma operation, the server programs collect data from the different devices described in the previous sections and stores it temporarily. In between shots, JET's central Control and Data Acquisition System (CODAS) connects to the server via an internal JET Ethernet connection and initiates a transfer of the data to a central database where it is stored in a Late Pulse File (LPF). The data acquisition is normally initialised by CODAS before each JET shot. However, an acquisition sequence can also be started from the DAQ PCs if desired.

The server programs handle the internal communication between the two DAQ PCs of the MPRu as well as the external communication with CODAS. The MPRu servers can be inquired by CODAS if they are ready to take data and what settings are used.

5.1.2 Data reduction'

The acquisition and storage of the full pulse shape for each registered TRC event allows post discharge processing. The MPRu data reduction chain consists of baseline restoration, gain correction, event separation and selection as well as background correction. The result is a time-resolved proton position histogram. The baseline restoration removes the effects of the applied voltage offset as well as any high and low frequency noise pickup from the individual pulse shapes. Since the different detector channels are affected by noise pick-up to a quite varying degree, each TRC data channel is analysed separately, and customised baseline restoration methods are selected for each channel individually. These methods include treating the baseline off-set as a constant, a linear or a sinusoidal function. The gain correction takes into account changes in signal amplification in the PMTs, PSAs and TRCs. It is based on a method using the YAP and LED light sources (22).

For event separation and selection, a two-gate Pulse Shape Discrimination (PSD) technique is used. Each waveform registered by the TRCs is divided into two parts ("gates"). The integrated charge, Q, is calculated for each part separately, i.e., for an early,""fast" part of the pulse, and a longer""slow" part after the fast gate. These sums of sampled voltage values are referred to as Q_{short} and Q_{long}, respectively, and constitute the basis for further event selection and separation as described

below. The storage of the full pulse shape gives the possibility to apply more advanced PSD techniques in the future.

Waveforms due to the CLS of the C&M system can be identified both by their timing within the plasma discharge, since these light sources are (in low rate operations) only activated before or after the main plasma pulse, and by their fixed repetition frequencies and characteristic pulse shapes. These latter properties make it possible to separate them also in situations where they are mixed with the normal scintillator events, such as would be the case if they were used to follow gain variations due to rate transients during a plasma pulse. This option will be studied in future high rate operations.

6 PERFORMANCE OF THE INSTALLED MPRU SYSTEM

6.1 CALIBRATION

The calibration (in energy and efficiency) of the MPRu depends on two sets of quantities. The first set is a number of physical relations and constants, namely, 2-body kinematics, nuclear masses (24), charged particle energy loss in matter (25), the Lorentz force and the double differential cross-sections (over energy and angle) for the H(n,p)n' reaction (26); these determine the physical process occurring in the spectrometer. The second set of quantities is that of the spectrometer, in terms of geometry, and magnetic field; these determine the response of the instrument to the physical process. All quantities are assembled into a response function calculation code (see Section 6.2.1), giving an *ab initio* (from first principles) calibration of the instrument.

The geometry of the magnetic system was measured by hand during assembly of the MPR in 1994-1995. The uncertainties of these measurements were estimated to <0.5mm. The internal geometry of the subsystems (conversions foils, proton collimator and neutron collimator) were determined with an uncertainty of 0.1-0.25mm. These uncertainties are the same for the MPRu. The magnetic field mapping was done at four different settings of the electromagnet, two close to the 2.5MeV setting and two for the 14MeV setting. Each magnetic setting was measured by Hall probes at more than 6000 points in the magnetic mid-plane. These measurements combined with the reference Hall probe measurements in the D1 and D2 poles are used to determine the magnetic field map for a specific magnetic setting. This determination involves an interpolation between the measured field maps, resulting in an interpolated field map. One such interpolated map corresponding to a setting for 2.5MeV neutron measurements is shown in Figure 3.

The geometry and alignment of the new components of the MPRu were surveyed during the assembly and installation in 2004-2005 using JET's digital photogrammetry system (16). The accumulated precision in the determination of the position of the focal plane detector with respect to the optical axis is about 0.1mm. Based on the dispersion (Table 6 below) this gives an absolute uncertainty of 0.2keV and 1.1keV in the energy determination in 2.5MeV and 14MeV operations, respectively. This precision contributes to a systematic uncertainty of $dE/E < 1 \cdot 10^{-4}$ in both cases. The total energy dependent neutron to proton conversion efficiency (ε) is given by:

$$\varepsilon_i = \Psi_{n,p,i} \cdot f_i \cdot d_i, \qquad (2)$$

where the index i denotes a specific setting of the MPR spectrometer, $\Psi_{n,p,i}$ is the total emission probability for recoil protons from np scattering to enter the proton collimator and f_i is their transmission from the proton collimator to the focal plane detector. Finally, d_i is the detector efficiency for protons of the scintillator array. Standard differential cross-sections for elastic H(n,p)n' scattering (26) are used for calculating $\Psi_{n,p}$ for the different energies and angles.

The error in the transmission stems mainly from the uncertainty in the geometry of the instrument and the implementation of this geometry into the response function code. The transmission has previously been calculated with another independent code giving consistent results; it is about 83% and 90% for 2.5 and 14MeV protons, respectively (see Table 6). The systematic error in the transmission results is estimated to be $k_{trans} \sim 2\%$. The number of particles in the simulation calculation is high enough to avoid a significant statistical contribution to the error.

The error in $\Psi_{n,p}$ comes from the uncertainty in the geometry of the target and the proton collimator and the uncertainty in the (n,p) cross section. The uncertainty in the geometry stems from a 0.1 mm uncertainty in the measurement of the target radius and the collimator diameters. This gives the following estimated errors for the reference 14MeV setting: the target area $k_{area} \sim 1.1$ %, the size of the solid angle of the proton collimator $k_{pcol} \sim 0.5$ % and the uncertainty in the thickness of the target $k_{target} \sim 1.0$ %. The uncertainty in the cross-section is $k_{c\text{-}s} \sim 1.4$ %. Assuming all errors to be Gaussian distributed and uncorrelated, the total error for the efficiency is 3%.

For the good resolution 2.5MeV setting (see Table 4) the estimated uncertainty in the target thickness is at present much higher, 6.5%. All other uncertainties are the same, which results in the total uncertainty in the efficiency for the setting to be 7%. For the high efficiency 2.5MeV setting the uncertainty in the target thickness is 3.1%, resulting in a total uncertainty in the efficiency of 4%. An estimate of the type of improvement that could be achieved with a better-known target thickness is here referred to as the *refined* setting, where the uncertainty in the target thickness has been set to 1% and all other values are as for the good resolution case. This hypothetical setting has a total uncertainty in the efficiency of 3%.

The response function code (see Section 6.2.1) is used to estimate the systematic uncertainties in σ/E_n and E_n by propagating the underlying uncertainties from the geometry. The geometrical uncertainties are assumed Gaussian distributed and uncorrelated. The error propagation is performed by executing the response function code 1000 times with added randomised errors to the geometrical input parameters (foil thickness, foil area, proton collimator radius and neutron collimator length). The widths of resulting distributions of σ/E_n and E_n represent their systematic uncertainties, $\Delta(\sigma/E_n)$, and ΔE. The results for the four different settings are summarised in Table 5.

The stability of the energy calibration depends on the stability of the spectrometer's magnetic field; this is monitored at a rate of 4Hz during plasma operation. The short- and long-term stability was verified at a reference setting for 2.5MeV neutron measurements where only small (sub Gauss) variations in the B-field were observed, both during the evolution of a pulse and over longer periods of operation. Over an 8 week period of JET operations in 2006 (500 plasma discharges), one of the

reference Hall probes showed a one-sigma spread of ±0.3G on a level of 3300G (the other was stable on a level of 4300G). This corresponds to an energy uncertainty of at most ±0.4keV, which is of the same order as the estimated uncertainty due to the positioning of the focal plane detector elements, and small compared to the mean neutron energy (of order 2450keV); it contributes a (random) uncertainty in the energy calibration of the order $dE/E \approx 2 \cdot 10^{-4}$ for a 2.5MeV setting.

6.2 Simulated spectrometer performance

Simulation codes were used for two main purposes. One was to include all the relevant knowledge about the full spectrometer system into a simulation code that could provide the spectrometer response functions. The second was to assist in the design and analysis of the new phoswich-based focal plane detector. The codes used for these two tasks are described in the following two sub sections.

6.2.1 Spectrometer response functions

All the inputs needed to assess the performance of the spectrometer were assembled into a Monte Carlo code used for calculating the instrumental response function. Protons are tracked from the conversion foil to the proton collimator and through the interpolated measured magnetic field using a fourth order Runge-Kutta technique. Validation of the response function was obtained from measurements with a point ^{241}Am source placed in the target position (8) and from fusion neutron measurements under specific conditions, in particular for ohmic plasmas (see Section 6.3.2). The response function is used both in the analysis of plasma neutron data and to provide information on spectrometer performance.

The response function of the spectrometer can be approximated by a number of (energy dependent) parameters. These include the dispersion along the detector array; the resolution of mono-energetic neutrons; the line shape, i.e., the proton position distribution at the detector array for one specific neutron energy (cf. line shapes of gamma spectrometers); the transmission fraction from proton collimator to detector array; and the overall efficiency.

The dispersion, resolution and line shape are illustrated in Figure 10 for typical 2.5MeV and 14MeV neutron measurement settings, where each proton position distribution over the detector plane is the result of a separate simulation calculation of mono-energetic neutrons that have been "forced" to scatter elastically in the conversion foil. Table 6 gives a summary of some of the performance parameters. The dispersion is the differential separation of proton energies over the length of the hodoscope, i.e., dE_p/dx. The transmission is the fraction of protons selected by the proton collimator that reach the detector array, which is about 97% efficient in registering protons (17). For the good resolution 2.5MeV operational point, the resolution (σ/E_n) of the spectrometer is 3.2% for mono-energetic protons of 2450keV. For 14MeV neutrons, the reference 14MeV operational point gives a resolution of 1.4% at 14.0MeV. The effective neutron collimator length is 870 mm in both cases.

6.2.2 Simulations of phoswich performance

To assist in the design of the instrument, interpretation of results and the evaluation of its performance, a separate Monte Carlo model has been set up specifically to study the performance of the phoswich scintillators of the detector array (27). The model is based on the GEANT4 code package (28) and includes the full geometry of the installed focal plane detector describing the detector assemblies as well as the mechanical support structures. The simulation calculates the response to signal protons as well as to the different background components like neutrons, gammas and electrons. The intensities and shapes of the background components were modelled using input from an analysis of the main 14MeV as well as the preliminary 2.5MeV measurements with the original MPR. The good resolution 2.5MeV setting and a 14MeV setting using a target thickness of 18mg/cm^2 was used in the simulations. The calculations can be done for any detector element of the hodoscope; here we report results for a central scintillator array channel. For the original MPR, 14MeV measurements in DT, the simulations gave a S/B = $2.5 \cdot 10^3$ while the experimental value was $2 \cdot 10^3$; for 2.5MeV measurements in D plasmas the simulations gave a S/B = $2.5 \cdot 10^{-1}$ while the experimental S/B was 10^{-1}. For the MPRu, the phoswich response was modelled with input from prototype tests using radioactive sources. In this case, the simulation predicts a 2.5MeV proton $S/B_{2.5} \sim 10$; in the 14MeV case the simulations predict a $S/B_{14} \sim 2.5 \cdot 10^4$. Note the predicted improvement factor of 40 in the 2.5MeV D plasma situation and 10 in the 14MeV DT plasma situation.

6.3 MEASURED SPECTROMETER PERFORMANCE

6.3.1 Signal to background determination

To evaluate the S/B of the MPRu experimentally, we have combined data from several hundred JET D plasma pulses where the spectrometer was operated at the 2.5MeV setting described in Table 6. This resulted in a data set containing both signal and background events; we call this the "signal+background" data set. The background component was determined from a separate data set where the magnet was turned off or set to 14MeV measurements; both these settings prevent 2.5MeV protons from reaching the detector array. It was tested if the background component seen by the MPRu in D plasma operations is affected by the level of the spectrometer's magnetic field, but no such effects were found.

The left frame of Figure 11 shows the Q_{short} versus Q_{long} distribution of a central detector channel for the signal + background data set. The black line in the figure indicates a "linear cut" applied to the (Q_{long}, Q_{short}) distribution. All events to the right of the cut are discarded and $Q_{tot} = Q_{short} + Q_{short}$ is calculated for the remaining events, resulting in the distribution shown in the right frame of Figure 11. In this Qtot distribution two regions are selected, namely, a normalisation region (between blue lines) and a signal region (between green lines). The normalisation region is assumed free from proton signal events. Data from the acquisition of background-only data (red points) are normalised to the signal+background data (black points) in the normalisation region. By subtracting the normalised background from the signal+background data in the signal region only signal events

remains and the total number of proton events in that region can be determined. For the central hodoscope detector shown here a S/B = 4.8 is obtained.

JET has not operated with DT plasmas since the installation of the MPRu, which has prevented us from measuring the S/B under these conditions. Instead, data from several hundred

JET pulses in D operations, using a 2.5MeV setting, were used to estimate the background level in the 14MeV region of a Q_{long},Q_{short} distribution (red rectangle of Figure 13). The total neutron yield of all JET pulses used in the background calculation is related to the total amount of protons reaching the hodoscope, using the efficiency and the installation geometry factor (see Section 5). Assuming a neutron energy distribution from a thermal plasma with ion temperature 10 keV, these data indicate that the reference 14MeV setting has a S/B = $1.4 \cdot 10^4$ for a central hodoscope channel.

6.3.2 Measurements

Data on the 14MeV neutron emission from Ohmically heated discharges in the DTE1 campaigns were used previously to validate the energy calibration of the MPR system (29). The new MPRu system is in this respect quite similar to the original MPR.

In Ref. (29), MPR Ohmic data for three different 14MeV settings have been analysed using a model with a single thermal (Gaussian) neutron emission spectrum corresponding to a fuel ion temperature of T_i = 2-3keV. No significant plasma rotation is expected in Ohmic operations. The combined results from the three data sets give a deviation of +0.8keV from the expected mean neutron energy of 14041 keV[8], well within the estimated systematic uncertainty of the energy calibration. At the time the systematic uncertainty was estimated to be ±20keV mainly from surveying (30). The surveying accuracy has been improved considerably in the MPRu installation and now contributes to ±1.4keV (see Section 6.1).

To validate the MPRu instrument in measurements of 2.5MeV neutrons in D plasmas, data were summed for (parts of) about 1500 JET Pulses from campaigns C15-C19 (2006-2007), when only Ohmic heating was applied. Due to the much lower neutron fluxes and somewhat lower efficiency of the system in D operations, the statistics is much reduced compared to the case with DT plasmas. The deduced mean neutron emission energy is 2465 ±9(stat) ±9(syst) keV, which is consistent with the expected neutron energy of 2458keV[9]. For this analysis, the thermal temperature was fixed at 2keV, based on the experience of Ohmic data from DTE1. The resulting fit gave a reduced $\chi^2 = 0.86$.

As an illustration of MPRu data for different heating scenarios, we present data from JET Pulse No: 68379 subjected to both Neutral Beam Injection (NBI) and ion cyclotron resonance heating (ICRH) and data from Pulse No: 68569 heated with NBI only. The total neutron yield was $3.5 \cdot 10^{16}$ and $6.0 \cdot 10^{16}$, for the mixed heating and NBI-only pulse, respectively.

The extracted proton position histograms are shown in Figure 12 together with the result of a preliminary analysis. Gaussian neutron energy spectra are convoluted with the response function and fitted to the two data sets for demonstration purposes. The intensity, width and mean energy of

[8] *For a "cold" DT plasma, E_n = 14028keV, to which is added a kinematical shift dependent on the plasma temperature. For a 2.5keV thermal DT plasma the shift is about 13keV (29).*

[9] *For a "cold" D plasma, E_n = 2449 keV, to which is added a kinematical shift dependent on the plasma temperature. For a 2 keV thermal D plasma the shift is about 9 keV (29).*

the Gaussians are free parameters of the fit. The fits to the data give a reduced χ^2 of 1.1 and 1.5 in the mixed and NBI-only cases, respectively. The best fit to the mixed heating pulse gives a broader neutron energy distribution than the NBI-only case (Figure 12c), namely, FWHM = 464 ±7 (stat) ±5 (syst) keV compared to 367 ±9 (stat) ±6 (syst) keV[10] (31). The broader neutron energy distribution in the mixed heating pulse reflects the fact that ICRH heating can accelerate the deuterium fuel ions up to several hundred keV of energy, while in the NBI case the maximum ion energy is given by the injection energy of the beams, here 130 keV. The analysis also indicates a common energy shift (beyond the kinematical shift discussed above) of about 40 keV for both data sets.

Even in D plasma operations tritium is present in the fusion device through the breeding reaction ($d + d \rightarrow t + p$). In a secondary reaction, these tritons can fuse with the bulk deuterium ions and thereby contribute a Triton Burn-up Neutron (TBN) emission. The intensity of the TBN emission in such plasmas is much lower (about 1% relative intensity) than the 2.5MeV neutron emission, but the TBN can clearly be seen when the MPRu is set to a 14MeV operational point during D operation. Data from a set of about 230 pulses when the MPRu was tuned to 14MeV measurements was combined to investigate the TBN component. Looking at the data for a single phoswich detector (Figure 13a), a concentration of events around (Q_{long}, Q_{short}) = (600, 600) is evident in the 14MeV data, but is absent when the system is tuned for 2.5MeV measurements (Figure 11a). This group of recoil protons is highlighted in the rectangular region indicated in Figure 13a (red line). Figure 13b shows the extracted proton position histogram, containing 3139 events, and the results of a preliminary analysis. The analysis used two spectral components, namely, a TBN component (black) of known shape, and a bulk component due to a population of residual tritium (4) (red dashed line) with a temperature assumed to 20keV. A fit to the data has been performed with three free parameters, namely, the intensity of the TBN component, and the intensity and mean energy of the thermal (Gaussian) component. The best fit to the data (blue), with a reduced $\chi^2 = 1.6$, is shown as lines in Figure 13b and the corresponding neutron energy spectrum is given in Figure 13c. The intensity of the residual tritium component is 9% of the total flux at the target, which is in fair agreement with previous results (4). Clearly, the TBN component alone would not give an acceptable fit to the data, illustrating the ability of the MPRu to discern multiple components even in situations of quite weak neutron emission.

The MPR is absolutely calibrated in flux efficiency, as discussed above. The measured MPRu 2.5MeV counts (integrated over full JET discharges) together with the absolute flux calibration of the instrument can be used to estimate the total JET neutron yield, Y. A separate estimate of the neutron emission profile is required, which can be obtained from an analysis of the JET neutron camera data. A preliminary comparison between the neutron yield of the MPRu, YMPRu, and that of the JET Fission Chambers (FC), Y_{FC}, has been performed for 311 JET discharges. The results are presented in Figure 14. A proportionality fit to the data gives $Y_{MPRu} = 1.06\ Y_{FC}$. This is consistent within the systematic uncertainty of the two systems. However, for the time period studied here, no processed neutron camera data was available and instead a fixed reference neutron emission profile

[10] *The relative systematic uncertainties of the width is calculated as $(R/W)^2\ (dR/R)$, where W is the FWHM of the neutron spectrum and R is the FWHM of the detector response (assuming a Gaussian response function).*

obtained from previous tritium campaigns was used for this preliminary analysis effort (32). The random uncertainties are dominated by the counting statistic in the MPR.

The highest count rate registered by the MPRu in JET D plasmas so far has been for Pulse No: 70232 with 800Hz when the total JET neutron rate was $1.8 \cdot 10^{16}$ n/s.

DISCUSSION

The limited range of JET operational scenarios offered since the installation of the MPRu in 2005 has not allowed experimental tests of all the relevant performance indicators of the spectrometer. Here we review some of these important aspects in view of the available experimental results using the simulations as an additional guide, with the aim to estimate the operational limits of the MPRu and identify possible areas for improvements.

The sensitivity of the MPRu has so far been tested in its ability to resolve the weak TBN component in D plasma operations. However, the data are still too scarce to make any detailed statements on the S/B in this measurement situation. In general, a high sensitivity is necessary in order to measure any weak components in the neutron emission. The sensitivity of the instrument is closely related to the S/B of the individual phoswich detectors and can be further improved by background corrections, within the limitations given by the counting statistics. The original MPR had a S/B of about $2 \cdot 10^3$ in 14MeV (target thickness =18mg/cm^2) (full DT) and 10^{-1} in 2.5MeV (full D) measurements. With phoswich detectors, double PMT read-out and event-based, digital TR electronics, simulations predict a S/B increase to $2.5 \cdot 10^4$ and 10 for the 14MeV and 2.5MeV cases, respectively (with the same settings). It is in this context interesting to mention that the GEANT4 simulations actually predict an improvement of a factor 40 in the 2.5MeV D plasma situation (see Section 6.2.2). The analysis presented above gave a MPRu $S/B_{2.5} = 5$ in 2.5MeV measurements, which is an improvement of a factor 50 with respect to the original MPR, consistent with the improvement factor predicted by the GEANT4 simulation. Based on D operations data, the present best estimation of the S/B_{14} is $1.4 \cdot 10^4$ with the reference 14MeV setting. Note, however, that the simulated S/B_{14} results was based on a setting using a 2.25 times thicker target. Scaling the simulated S/B_{14} with this factor results in a higher estimated S/B14 than simulations predicted, corresponding to an improvement factor of about 16. The original MPR could distinguish weak components down to the 10^{-4} level of the main emission (1); consequently, the MPRu should be able to push the sensitivity to about 10^{-5}, statistics permitting.

We estimate that the main rate capability limitation with the system still lays with the individual detector channels, in particular the performance variations of the PMTs associated with high and variable event rates. However, with the performance monitoring offered by the C&M system of the MPRu, making tracking of transients during a plasma pulse possible, we estimate that individual scintillators should be able to sustain rates of several hundred kHz with preserved data quality. This would indicate a maximum useful count rate in the full spectrometer of several MHz.

The energy bite of the present MPRu is restricted to $E_0 \pm 20\%$ by the physical dimensions of the

focal plane detector and the properties of the spectrometer's magnetic field. In principle, the tunable B-field makes it possible to measure neutrons in a broad range of energies, not only around the dominant 2.5 and 14MeV neutron emission bands, but actually at any energy from 0 to 20MeV. In practice, the more severe background situation encountered at lower neutron energies would restrict the possibilities to $E_n > 1$MeV.

The dynamic range of the MPRu in terms of plasma fusion neutron rate varies depending on the plasma conditions. Under certain conditions, a relatively modest instrumental resolution is sufficient, in which case the efficiency of the system can be increased and consequently the operating range can be pushed towards lower neutron rates. In other cases, time-resolved results with good energy resolution are needed, requiring higher neutron rates. For the sake of illustration, as a miniumum requirement we consider the determination of a 20keV ion temperature with 10% precision and 1 second time resolution using the MPRu with a 1.8% and 3.3% energy resolution setting (for 14MeV and 2.5MeV measurements respectively). To achieve this (33), 400 protons per second are required in 14MeV operations, which implies a minimum JET neutron rate of about $4 \cdot 10^{15}$ neutrons per second. For 2.5MeV operations, 300 protons are required and the minimum rate is about 10^{16} neutrons per second. The high end rate is set by the individual detector channels abilities to cope with high count rates. For the present phoswich assemblies this is about 200 kHz per scintillator, which translates to about 2MHz for the full detector and further to a total JET flux of 10^{22} 14MeV neutrons per second (employing the thinnest conversion foil, the longest neutron collimator and the most restrictive proton aperture presently available, i.e., the lowest possible efficiency). Thus, for the present MPRu in 14MeV measurements, the dynamic range is about $2 \cdot 10^6$ ($4 \cdot 10^{15} < R_n < 10^{22}$), with an estimated $S/B = 2 \cdot 10^4$ at the low-rate end.

The uncertainty of the target thickness in the good resolution 2.5MeV setting is 6.5%. This uncertainty can be reduced by a cross-calibration with the better-known thickness of the 2.76-mg/cm^2 target and in a post mortem analysis by measuring the foil thickness with better accuracy.

The systematic uncertainties of the MPRu are decreased compared to the original MPR. This reduction is mainly due to the increased precision of the surveying of the spectrometer. The estimated systematic uncertainty of the energy calibration in the good resolution 2.5MeV and reference 14MeV setting is 9keV and 3keV, respectively. These uncertainties correspond to toroidal plasma rotations of 60km/s and 8km/s (23) (34). The estimated systematic uncertainty of the refined 2.5MeV setting is 1.5 keV, which corresponds to a toroidal rotation of 10km/s.

The estimated systematic uncertainty of the width of a neutron spectrum is small for both the 2.5MeV and the 14MeV settings. The systematic and the statistical uncertainties of a 2keV D plasma are of the same magnitude when the number of proton counts is $3 \cdot 10^2$ for the good resolution 2.5MeV setting and 10^4 for the refined 2.5MeV setting, corresponding to 10^{16} and 10^{17} JET neutrons, respectively. The systematic and statistical uncertainty of the measured width of a 2keV DT plasma are of the same size when 10^4 protons (10^{17} JET neutrons) are detected, using the reference 14MeV setting.

8. OUTLOOK

An important aspect of the modular structure of the MPRu concept is that it allows for improvements of specific sub-systems, without a complete re-build of the entire instrument. For example, the focal plane detector is easily removed and replaced, allowing for improvements based on progress in detector techniques. The present selection of a phoswich hodoscope offers good performance in a broad range of neutron (proton) energies; however, a selection of detectors that are more optimised for a more restricted energy range is always a possibility (as was indeed the case in the original MPR). Furthermore, the present restriction to 6 conversion foils and 5 proton apertures could be removed in a different design.

The light collection efficiency of the phoswich detectors could be improved, partly by selecting scintillating materials for the thin and thick layers that are more optimally matched, partly by improving the quality of material interfaces (35). Based on initial measurements on a prototype detector, we conclude that an improvement of about a factor of 2 is possible (36). The electronic and pick-up noise seen by the individual TR channels at JET is more severe than was observed in laboratory tests, both in terms of magnitude and structure, and the correction for this introduces a slight deterioration of the S/B. To reduce the impact of the noise, PMTs with higher gains can be employed or the amplitude of the signals can be increased by adding new amplifiers. This would simplify the analysis and reduce the errors introduced in the baseline restoration. Finally, by increasing the width of the neutron collimator it would be possible to increase the flux at the foil and hence reduce the minimum requirement of neutron yield to perform neutron spectroscopy; a wider neutron collimator would also increase the S/B ratio and reduce the errors in the yield determination.

Refinements in the topology of the B-field could be made using modern magnetic simulation codes, thereby increasing the energy bite to some extent; the corresponding modifications of the detector array would be a comparatively trivial task.

Since the neutron yield measurements of the MPRu are absolutely calibrated, they can be used in a comparison with data from other instruments and simulation from, e.g., TRANSP (37).

CONCLUSION

The MPR neutron spectrometer has been upgraded and the performance improvements in signal to background are in line with project goals and expectations from simulations. With the upgrade, the instrument can perform neutron spectroscopy in both pure D and DT plasmas and thereby provide valuable information on the physics of the fusion plasma in all experimental scenarios. The MPRu can benchmark codes and fine-tune experimental settings in a D phase. Hence, the instrument is ready to deliver high quality data from day one of the next JET DT experiment. This feature is also important for the ITER experiment since reliable neutron data is essential from the start of ITER DT experiments.

From the data collected in D plasmas one can project the instrument is performance in DT operation to give a S/B = $1.4 \cdot 10^4$ and a rate capability in excess of 1MHz. Hence, the fast ion

population from RF heating, NB heating and alpha knock-on reactions can be studied in even more detail. In JET D operation the instrument can provide complementary spectroscopic information (34) together with other spectrometers, e.g.,TOFOR (38).

The original MPR showed that the technique could provide an estimate of the total JET 14MeV neutron yield with low systematic uncertainties (32), and with the MPRu these measurements are further improved. The results of the MPRu achieved on JET shows that the instrument can also measure the 2.5MeV neutron yield. The ability to distinguish between the D and the DT neutron emission makes the instrument an excellent candidate for detailed studies of the two species in scenarios where they are both present, such as in trace tritium experiments[11] and during the advanced ITER D phase.

ACKNOWLEDGMENTS

This work has been performed under the European Fusion Development Agreement (EFDA) and the Association EURATOM-VR with support from Swedish Research Council, Uppsala University and JET-EFDA. The views and opinions expressed herein do not necessarily reflect those of the European Commission. A special thanks to Olle Byström for providing drawings and to Garry Kaveney for all the help with installing the MPRu at JET.

REFERENCES

[1]. *Observation of the Alpha Particle "Knock-On" Neutron Emission from Magnetically Confined DT Fusion Plasmas*. Källne, J. et al. 2000, Phys. Rev. Lett., pp. 1246-1249.

[2]. *Systematic spectral features in the neutron emission from NB heated JET DT plasmas*. Henriksson, H. et al. 2005, Plasma Phys. Control. Fusion, Vol. **47**, pp. 1763–1785.

[3]. *Synergetic RF and NB heating effects in JET DT plasmas studied with neutron emission spectroscopy.* Henriksson, H. et al. 2006, Nucl. Fusion, Vol. **46**, pp. 244–253.

[4]. *Triton burn-up neutron emission in JET low current plasmas*. Sjöstrand, H et al. 2008, J. Phys. D: Appl. Phys, Vol. **41**, p. 115208. 11 Experiments where the tritium levels are below 10%.

[5]. *Nuclear performance of the D-D phase of ITER*. Khripunov, V. 2000, Fusion Engineering and design, Vols. **51-52**, pp. 281-287.

[6]. *Neutron Spectrometry at JET (1983-1999).* Jarvis, O N. 2002, Nucl. Inst. and Meth., Vol. **A476**, pp. 474-484(11).

[7]. *Magnetic proton recoil spectrometer for fusion plasma neutrons*. Källne, J. and Enge, H. 1992, Nucl. Instr. and Meth. **A311**, pp. 595-602.

[8]. *Neutron emission spectroscopy at JET—Results from the magnetic proton recoil spectrometer.* Ericsson, G., et al. 2001, Rev. Sci. Instr., Vol. **72**.

[9]. *New neutron diagnostics with the magnetic proton recoil spectrometer.* Källne, J. et al. 1999, Rev. Sci. Instr., Vol. **70**, p. 1181.

[11] *Experiments where the tritium levels are below 10%.*

[10]. *The monitoring system of a high performance fusion neutron spectrometer.* Tardocchi, M. et al. 2002, Nucl. Instr. and Meth., Vol. **A485**, pp. 624–639.

[11]. *Study of signal to background ratio in fusion neutron spectroscopy measurements at JET for next step tokamak applications*. Hjalmarsson, A. 1999. UU-NF 99/#7.

[12]. *Upgrade of the Magnetic Proton Recoil (MPRu) spectrometer for 1.5-18 MeV neutrons for JET and the next step*. Ericsson, G. et al. 2006. Proceedings of Science FNDA.

[13]. *New MPRu instrument for neutron emission spectroscopy at JET.* Sjöstrand, H. et al. 2006, Rev. Sci. Instr., Vol. **77**, p. 10E717.

[14]. *Annual Report of the EURATOM/UKAEA Fusion Programme 2004/05*.

[15]. *Radiation detection and measurements*. Knoll, G.F. New York : Wiley, 1999.

[16]. The basics of photogrammetry. *Geodetic Services Inc*. [Online] **29** 9 2005. [Cited: 14 01 2008.] http://www.geodetic.com/Whatis.htm.

[17]. Glasser, W. *Determination of the hodoscope geometry of the MPRu neutron spectrometer.* 2005. http://www.inf.uu.se/Reports/UU-NF05-11.html.

[18]. MCNP home page. [Online] http://mcnp-green.lanl.gov/.

[19]. *A PCI transient recorder module for the JET magnetic proton recoil neutron spectrometer.* Combo, A. et al. 2004, Fusion Engineering and Design, Vol. **71**, pp. 151-157.

[20]. *Control and monitoring system for fusion neutron spectroscopy on the Joint European Torus*. Tardocchi, M. et al. 2004, Rev. Sci. Instrum., Vol. **75**.

[21]. *A Bipolar LED drive technique for high performance stability and power in the nanosecond time scale*. Ronchi, E. et al. 2009, Nucl. Inst. and Meth., Vol. **A599**, pp. 243–247.

[22]. *Control and Monitoring System of the Upgraded Magnetic Proton Recoil Neutron Spectrometer at JET.* Sjöstrand, H., et al. 2008, EFDA-JET-Preprint(08)07.

[23]. *Ion temperature and plasma rotation profile effects in the neutron emission spectrum*. Tardocchi, M. et al. 2004, Rev. Sci. Instr., Vol. **75**, pp. 661-668.

[24]. http://nucleardata.nuclear.lu.se/database/masses.

[25]. http://physics.nist.gov/PhysRefData/Star/Text/PSTAR.html.

[26]. CNS Data Analysis Center. [Online] [Cited: 20 2 2008.] http://gwdac.phys.gwu.edu/.

[27]. *Performance studies of phoswich detectors in the upgraded Magnetic Proton Recoil neutron spectrometer.* Wikström, G. 2005. UU-NF 05/#01.

[28]. Geant4: A toolkit for the simulation of the passage of particles thorugh matter. [Online] [Cited: 20 2 2008.] http://geant4.web.cern.ch/geant4/.

[29]. *Neutron Spectroscopy Studies of Heating Effects in Fusion Plasma*. Henriksson, H. 2003. PhD thesis. ISSN: 1104-232X ISBN: 91-554-5678-2.

[30]. *Neutron emission study of DT plasmas heated with tritium neutral beams*. Henriksson, H. et al. 2001, Rev. Sci. Instr., Vol. **75**, p. 832.

[31]. *On ion temperature profile measurements in ITER by means of neutron spectroscopy.* Elevant, T. et al. 1995. JET-P(95)65.

[32]. *Fusion power measurements using a combined spectrometer-camera system at JET.* Sjöstrand, H., et al. EDFA-JET-PR(08)02.

[33]. *Neutron measurement techniques for tokamak plasmas.* Jarvis, O.N. 1994, Plasma Phys. Control. Fusion, Vol. **36**, p. 209.

[34]. *Validating TRANSP simulations using neutron emission spectroscopy with dual sight lines.* Hellesen, C. et al. Rev. sci. Instr., Vol. **79**. In print.

[35]. *Test Of Phoswich Scintillators For The MPRu Neutron Spectrometer.* Hellesen, C. 2005. http://www.inf.uu.se/Reports/UU-NF05-03.html.

[36]. *Development and characterization of the proton recoil detector for the MPRu neutron spectrometer.* Giacomelli, L. et al. 2006, Rev. Sci. Instr., Vol. **77**, p. 10E708.

[37]. Ongena, J. 1998, Trans. Fusion Technol. , Vol. **33**, p. 181.

[38]. *The 2.5-MeV neutron time-of-flight spectrometer TOFOR for experiments at JET.* Gatu Johson, M. et al. 2008, Nucl. Instr. and Meth., Vol. **A591**, pp. 417-430.

Foil	1	2	3	4	5	6
Thickness (mg/cm^2)	1.58	2.76	3.67	8.09	13.6	22.1

Table 1: The thickness of the six conversion foils presently installed in the MPRu. All foils have a 10 cm^2 active area.

Position	Type	Radius (mm)	Solid Angle (msr)
1	Circular with cross hair	34.9	39.5
2	Triangular	Special	Special
3	Circular	40.0	51.9
4	Circular	34.9	39.5
5	Circular	18.0	10.5

Table 2: The five different proton collimator apertures of the MPRu. An approximate solid angle is given, as seen from the centre of the conversion foil. The triangular opening is used for calibration and tuning of the instrument.

Type	#	Position	Light Guide Shape	Thickness of layer			Width (mm)	Length (mm)
				Fast BC404 (mm)	Slow BC444 (mm)	Backing BC800 (mm)		
III	9	Low Energy	Straight	0.3	2.3	1.3	20	100
IV	7	Mid Energy	Bent (against)	0.3	2.5	5.0	10	100
V	6	Mid Energy	Bent (from)	0.3	2.5	5.0	10	100
VI	10	High Energy	Straight	0.3	3.2	0.0	20	100

Table 3: Specifications for the four types of phoswich scintillators and their nominal dimensions. The second column gives the number of items of each scintillator type present in the detector. The light guide shapes are either straight or bent. The bent light guides are bent either away from or towards the electromagnet.

E_n [MeV]	Setting name	Proton Collimator radius [mm]	Foil thickness [mg/cm^2]	Efficiency [10^{-6}]	Resolution (σ / E_n) [%]
14		18.0	3.67	0.51	0.83
		18.0	8.09	1.1	1.0
	Reference	34.9	8.09	5.2	1.42
		34.9	13.6	8.7	1.7
		40.0	8.09	6.5	1.6
		40.0	13.6	11	1.8
2.5	Good resolution	40.0	1.58	4.4	3.3
	High efficiency	40.0	2.76	7.6	5.4

Table 4: The combinations of proton collimator radius and foil thickness closest to the simulated optimal combination for 14MeV (DT) and 2.5MeV (D) measurements. Efficiency and resolution values are given for mono-energetic neutrons of 2.5MeV and 14.0MeV, respectively.

E_n	2.5 MeV			14 MeV
Setting name	Good resolution	High efficiency	Refined	Reference
$\frac{\Delta s}{s}$	7 %	4 %	3 %	3 %
$\sigma/E_n \pm \Delta(\sigma/E_n)$	3.3 % ± 0.2 %	5.4 % ± 0.1 %	3.30 % ± 0.03 %	1.42 % ± 0.01 %
ΔE	8.6 keV	4.8 keV	1.4 keV	3.1 keV
$\Delta E/E_n$	0.4 %	0.2%	0.06 %	0.02 %

Table 5: The estimated systematic uncertainty of the efficiency, the resolution and the energy calibration. The refined setting is a hypothetical 2.5MeV setting, using the same nominal setting values as the good resolution 2.5MeV setting, with an uncertainty in the target thickness of 1% instead.

	2.5-MeV operational point				14-MeV operational point			
Neutron energy (E_n) [keV]	2 250	2 450	2 750	2 950	12 600	14 000	15 400	16 800
Median position [mm]	89.5	198.6	355.2	450.8	128.6	261.2	383.2	494.5
Dispersion [keV/mm]	3.27	1.82	1.99	2.13	10.2	10.9	11.9	13.1
σ [keV]	99.1	79.1	76.1	75.8	194.7	199.5	218.2	241.6
Resolution (/E_n)[%]	4.4	3.3	2.8	2.6	1.5	1.4	1.4	1.4
Transmission [%]	81.5	83.1	81.2	78.4	91.3	90.3	87.6	83.1

Table 6: Simulation results for the good resolution 2.5MeV and the reference 14MeV operational point. The spectrometer settings are described in the text.

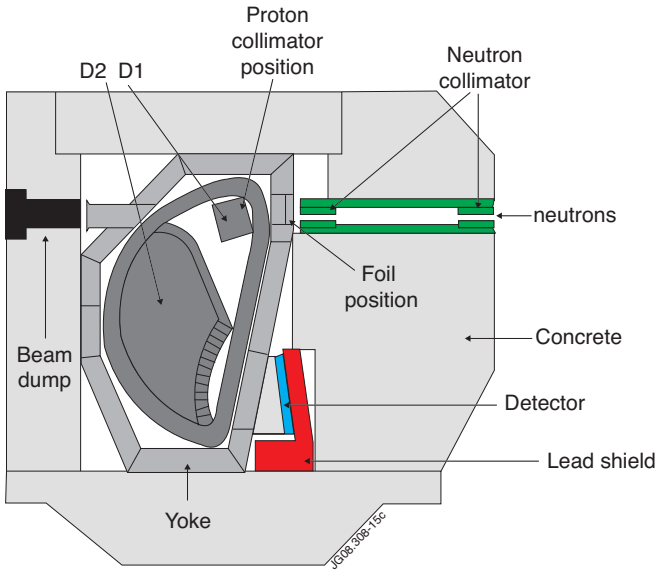

Figure 1: Vertical cut through the MPRu with its radiation shield.

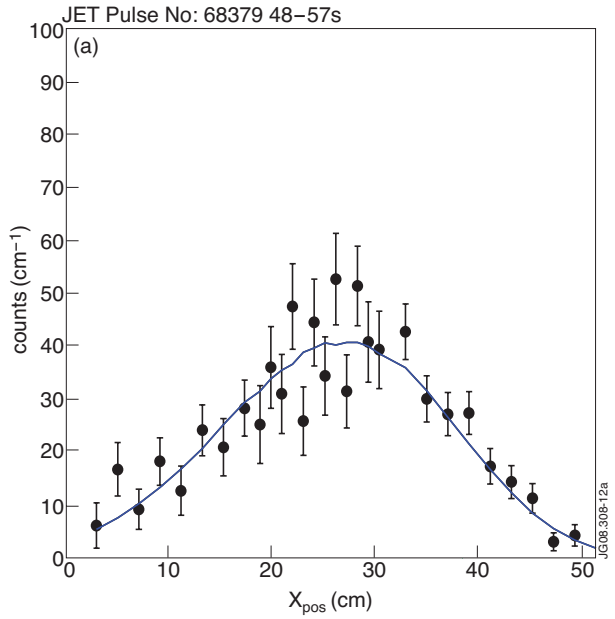

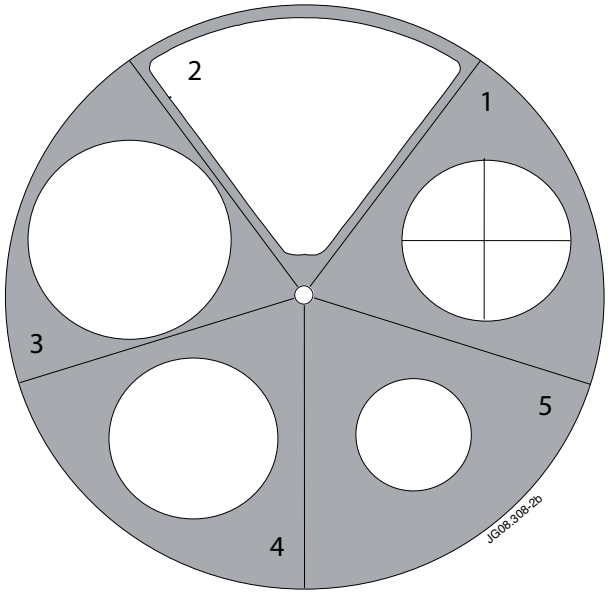

Figure 2: Conversion foil and proton aperture arrangements. Left panel: Photograph of the conversion foil holder, made from graphite and aluminium. "A" points to one of the CH_2 foils, "B" to a graphite holder , "C" to the Al base plate, and "D" to the crosshair and central hole in position 6, to the right of foil "A". Right panel: Schematic drawing of the five available apertures of the proton collimator. Note the cross hair in proton collimator position 1.

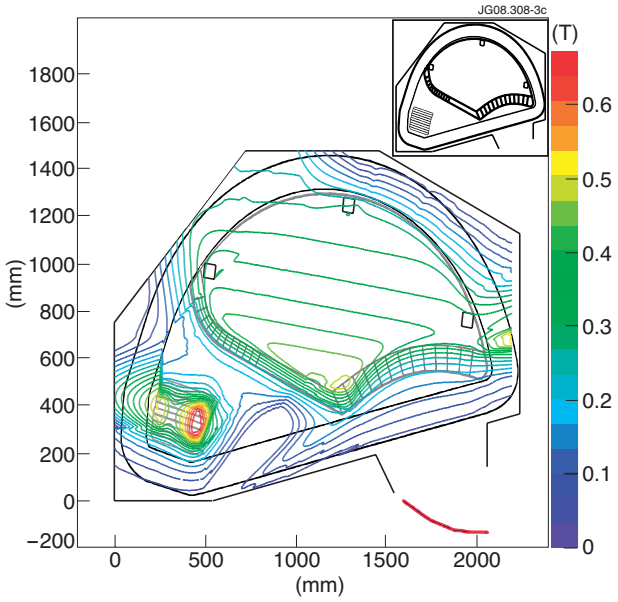

Figure 3: Interpolated magnetic field map of the MPRu for a 2.5MeV setting in the magnetic symmetry plane. The x and y axes are both in mm and the contour lines give the magnetic field strength. Indicated in the figure are the positions of the inner wall of the yoke and the outline of the coils (black), the magnetic poles (grey) and the curved focal plane (red). Three distance blocks (black squares) in the D_2 pole are also indicated; these were used as reference points in the surveying of the instrument. The insert shows the same geometry without the magnetic field map.

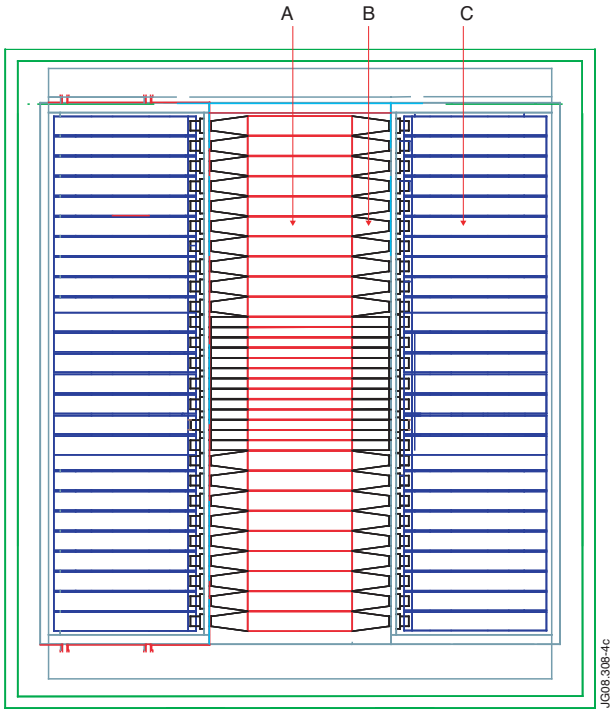

Figure 4: The layout of the MPRu focal plane detector array. Shown are the phoswich scintillators in the centre (red outlines; A), the light guides (black; B), the PMT assemblies (blue; C), and the surrounding mounting frame (green).

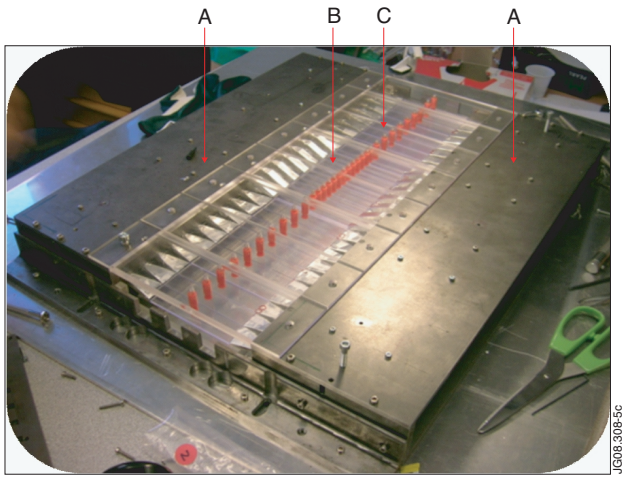

Figure 5: Overview of detector mechanics, with the PMTs mounted inside their magnetic shield boxes (A). The plastic roof (B) and the fibre guides pieces (C) are also visible.

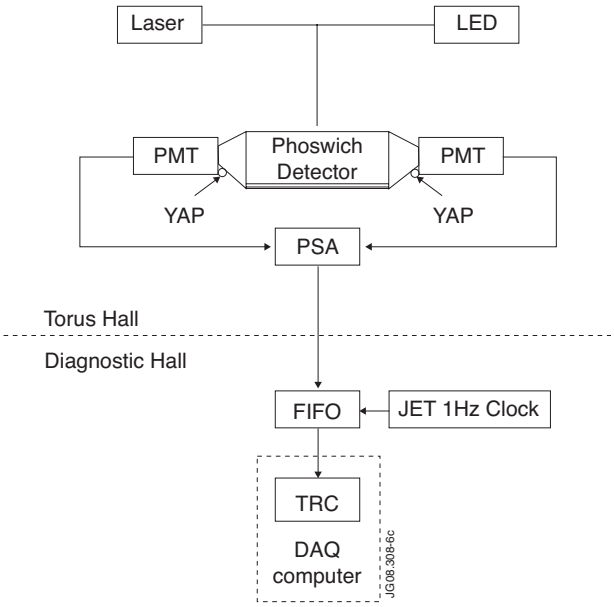

Figure 6: Overview of signal chain for channel 0, where dashed lines and whole lines are optical and electrical connections, respectively. All other channels have the same signal chain, but do not include the YAP sources, the FIFO and the JET 1 Hz clock.

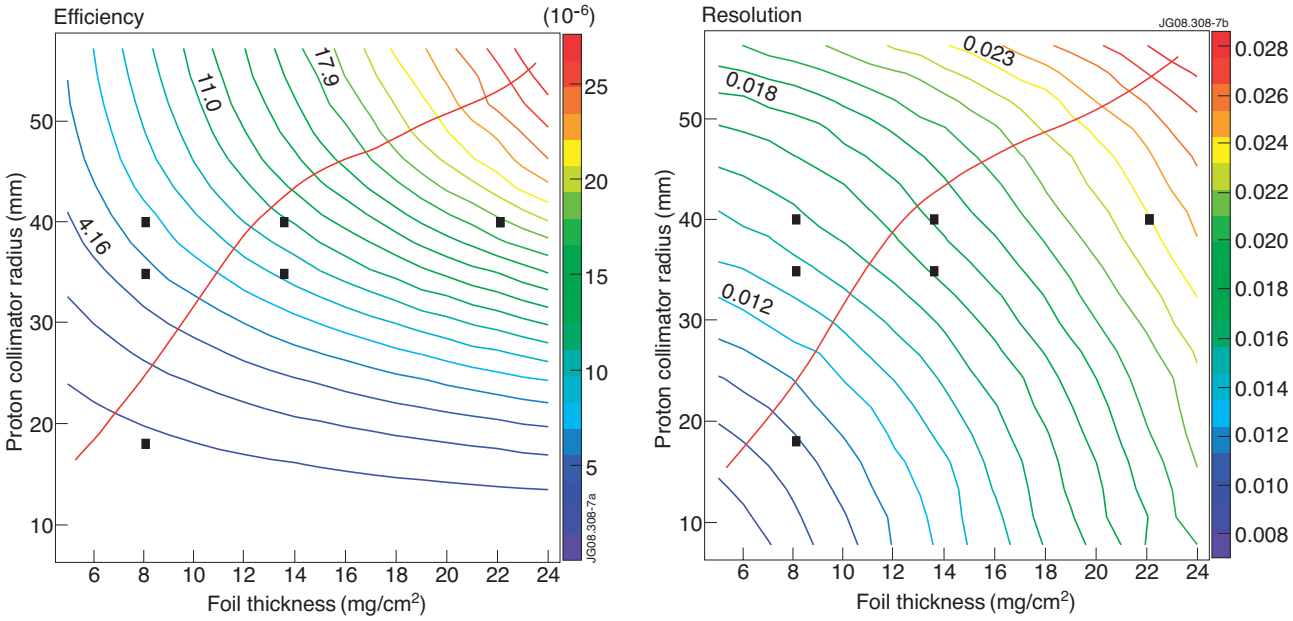

Figure 7: Optimisation of spectrometer settings for 14MeV operations. Left frame: The efficiency of the MPRu as a function of proton collimator radius and foil thickness. Right frame: The resolution (σ/En) of the MPRu as a function of proton collimator radius and foil thickness. Black squares in the figures refer to the possible MPRu settings for the proton collimator and the foil target.

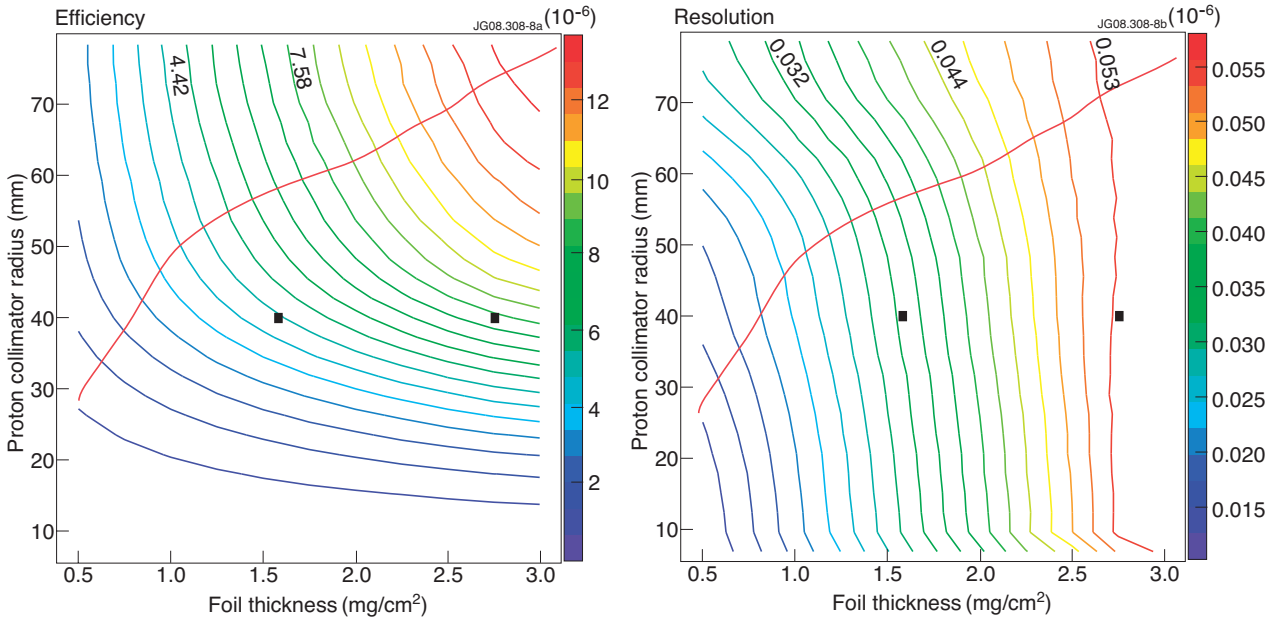

Figure 8: Same as for Figure 7, but for mono-energetic 2.5MeV neutrons.

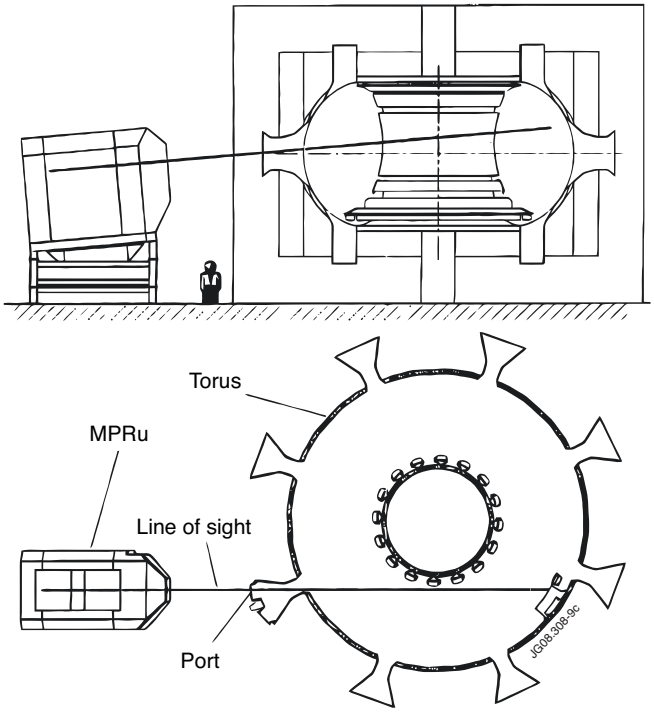

Figure 9: Illustration of the semi-tangential LOS of the MPRu.

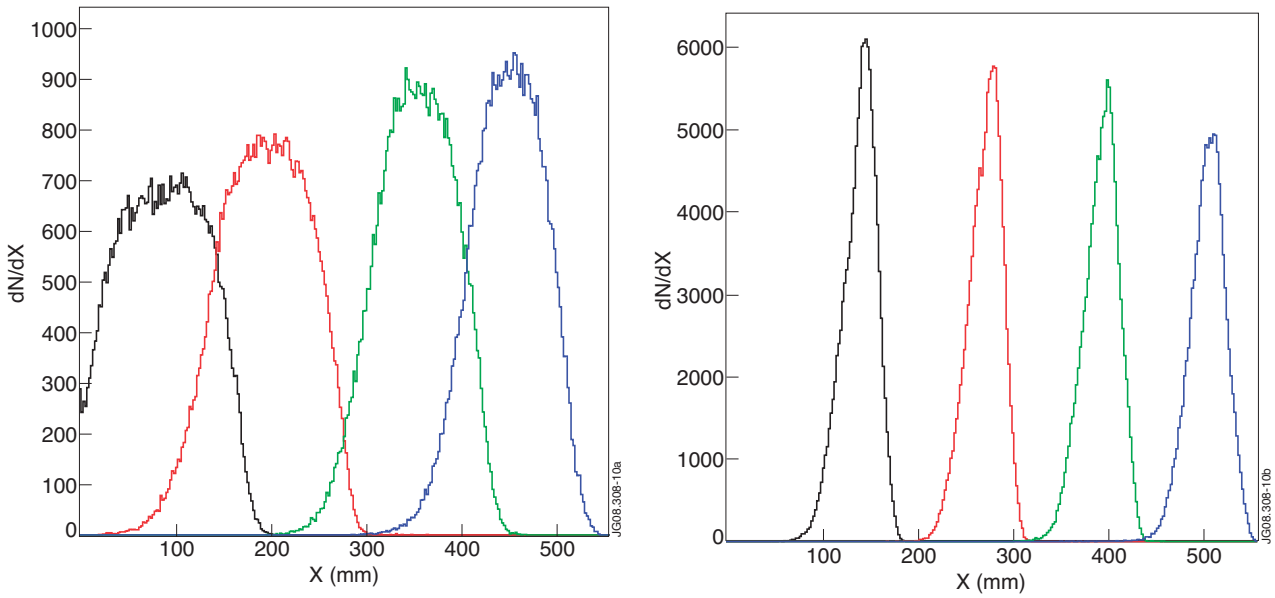

Figure 10: Simulated proton position distributions at the focal plane detector. The left frame shows results for four cases of mono-energetic neutron emission for the 2.5MeV operational point of Table 6, namely, 2.25MeV (black), 2.45MeV (red), 2.75MeV (green) and 2.95MeV (blue). The right frame shows results for four mono-energetic cases for the 14MeV operational point of Table 6, namely, 12.6MeV (black), 14.0MeV (red), 15.4MeV (green) and 16.8 MeV (blue).

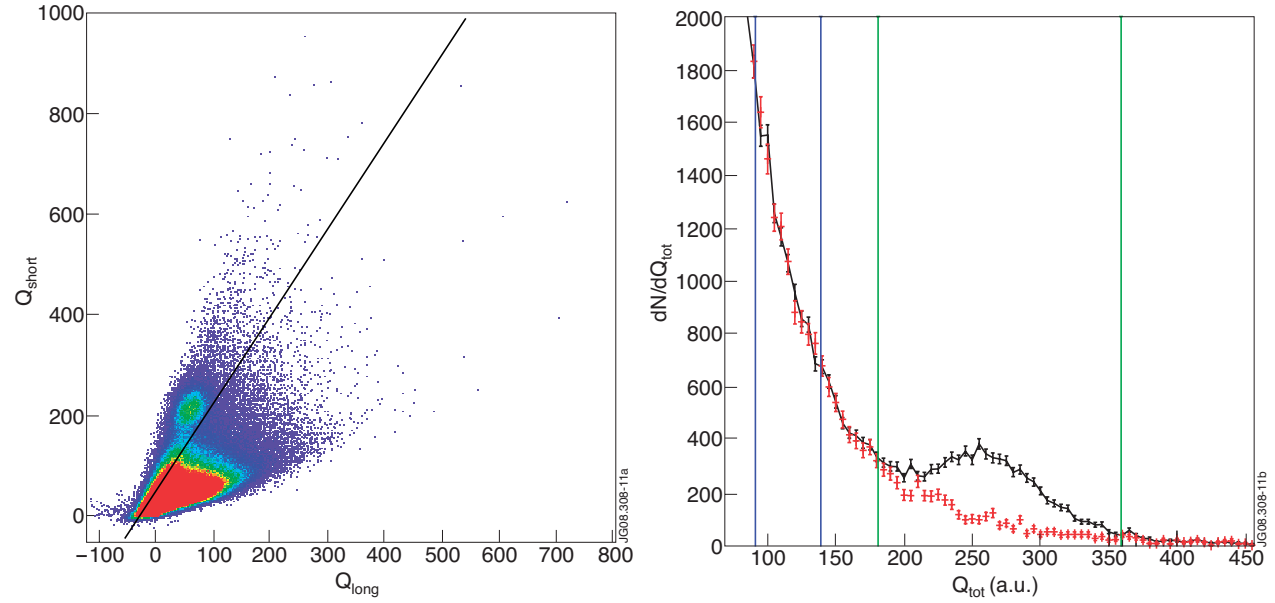

Figure 11: Left frame: The 2.5MeV signal+background data for a typical central hodoscope channel as a function of Q_{long} (x-axis) and Q_{short} (y-axis). The black line indicates the linear cut mentioned in the text. Right frame: Signal+background (black points and line) and scaled background (red points) of a central channel. The histogram shows the number of counts in a central channel as a function of Q_{tot}. The two blue (two left-most vertical) and two green (two right-most vertical) lines enclose the normalisation and signal regions, respectively.

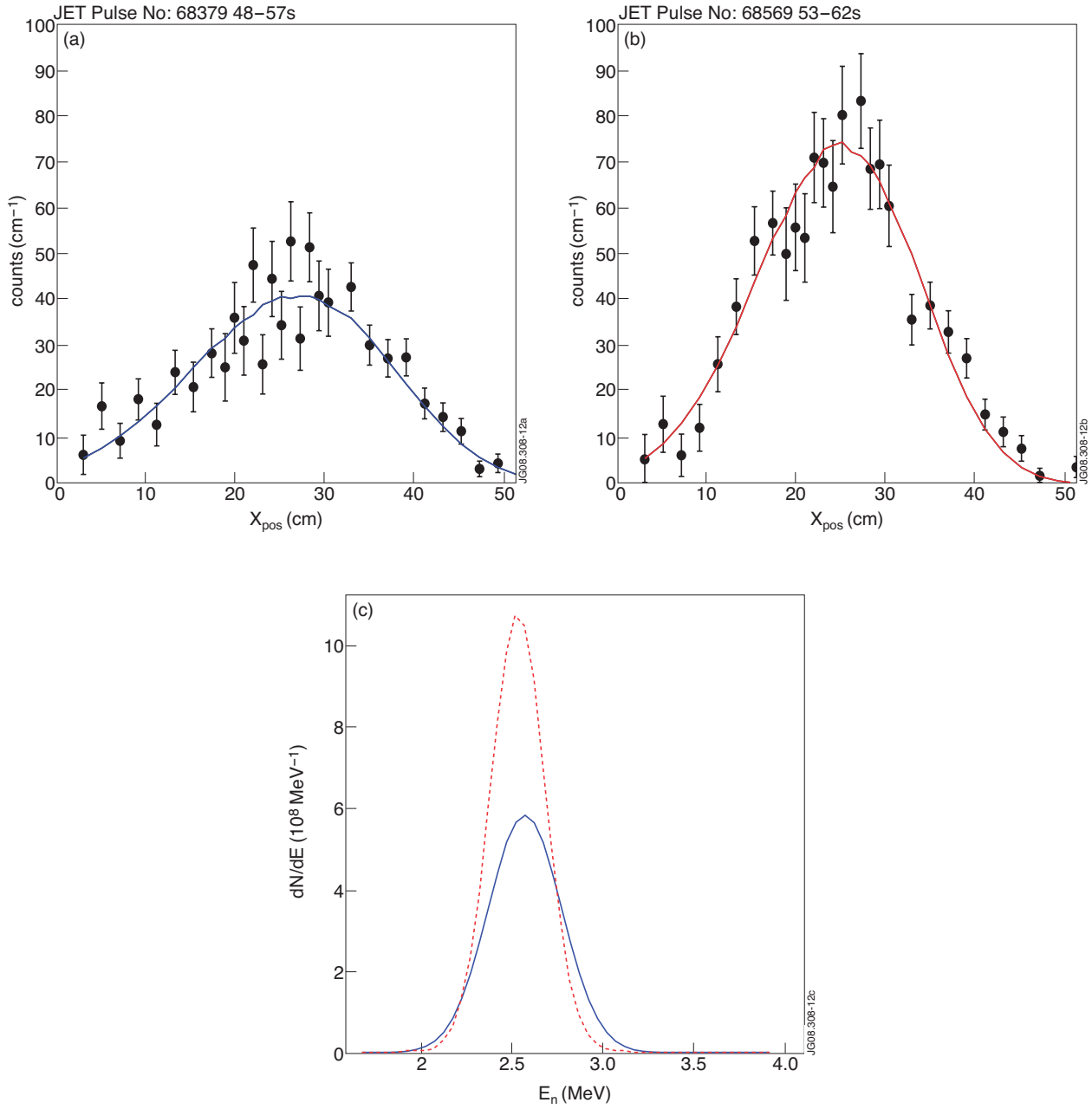

Figure 12: (a) Proton position histogram for Pulse No: 68379, which was heated with both NB and ICRH, including the result of a preliminary analysis (blue solid line). (b) Proton position histogram for Pulse No: 68569, which was heated with NB only, including the analysis result (red solid line). (c) Energy spectra (Gaussian) corresponding to the best-fit parameters for Pulse No: 68379 (NBI+ICRH, blue solid line) and Pulse No: 68569 (NB, red broken line).

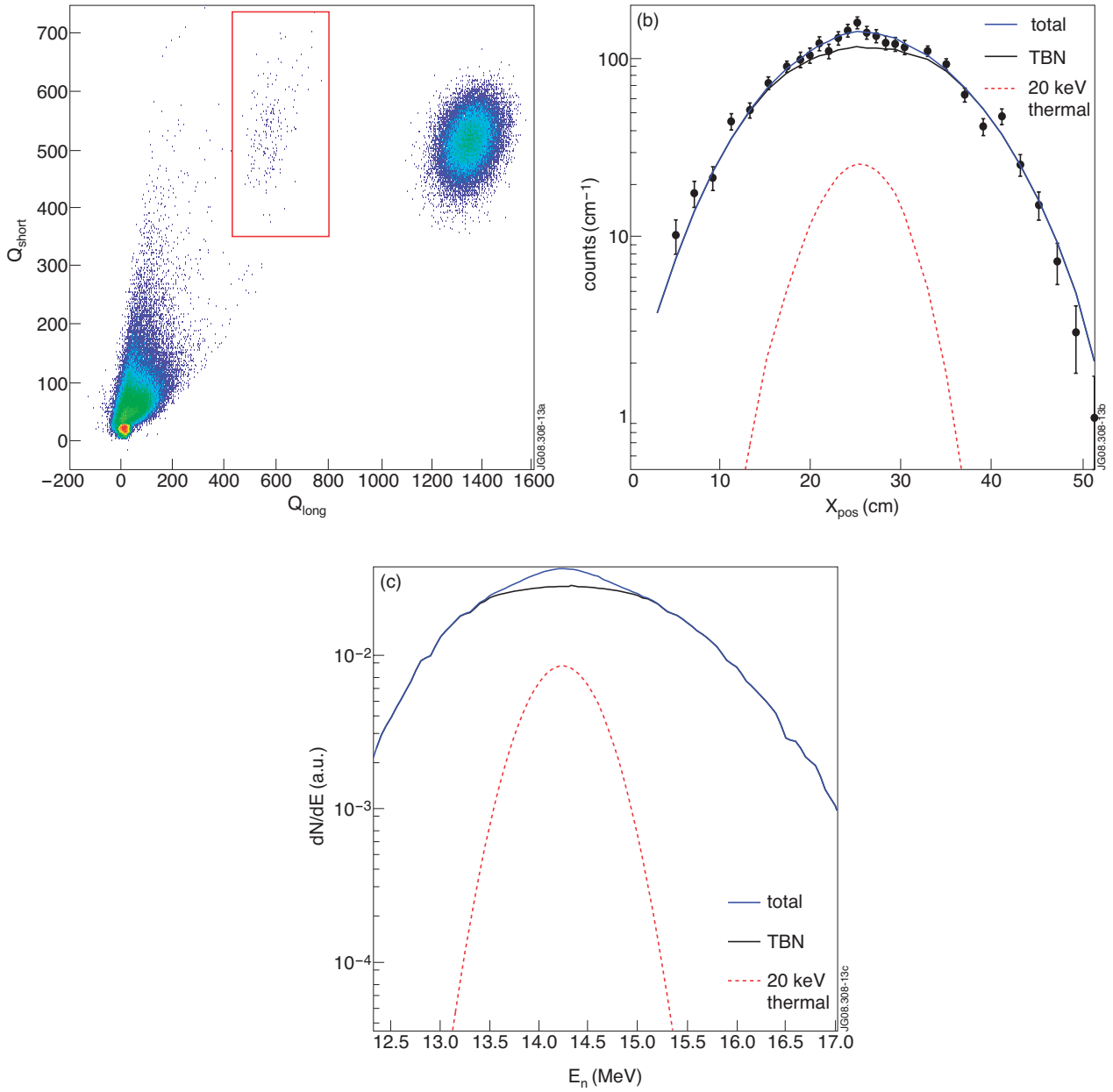

Figure 13: Illustration of 14MeV measurements during D plasma operation (data from JET Pulse No's: 69481-69718). (a) Q_{short} versus Q_{long} distribution in a single central phoswich detector channel; the rectangle encloses the selected "14MeV" proton events. The events at about Q_L,$Q_S \approx 1400$,500 are due to the C&M LED. (b) Position distribution of selected proton events from all detector channels (except channel 21), with the best-fit result drawn as full and dashed lines (see text for details). (c) The neutron energy spectrum corresponding to the best-fit case shown in b).

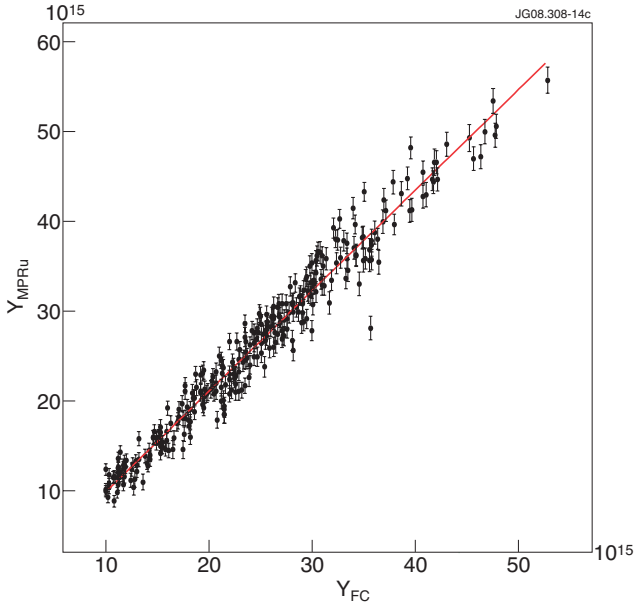

Figure 14: The neutron yield estimated with the MPRu compared to the result of the calibrated fission chambers.